Supporting Information

Antiferromagnetic exchange and long-range magnetic ordering in the supramolecular networks constructed of hexacyanido-bridged Ln^{III}(3-pyridone)–Cr^{III} (Ln = Gd, Tb) chains

Szymon Chorazy,*[a] Michał Rams,[b] Maciej Wyczesany,[a] Koji Nakabayashi,[c] Shin-ich Ohkoshi,*[c] and Barbara Sieklucka[b]

[a] *Faculty of Chemistry, Jagiellonian University, Gronostajowa 2, 30-387 Kraków, Poland.*
[b] *Institute of Physics, Jagiellonian University, Łojasiewicza 11, 30-348 Kraków, Poland.*
[c] *Department of Chemistry, School of Science, The University of Tokyo, 7-3-1 Hongo, Bunkyo-ku, Tokyo 113-0033, Japan.*

*Corresponding authors: chorazy@chemia.uj.edu.pl; ohkoshi@chem.s.u-tokyo.ac.jp.

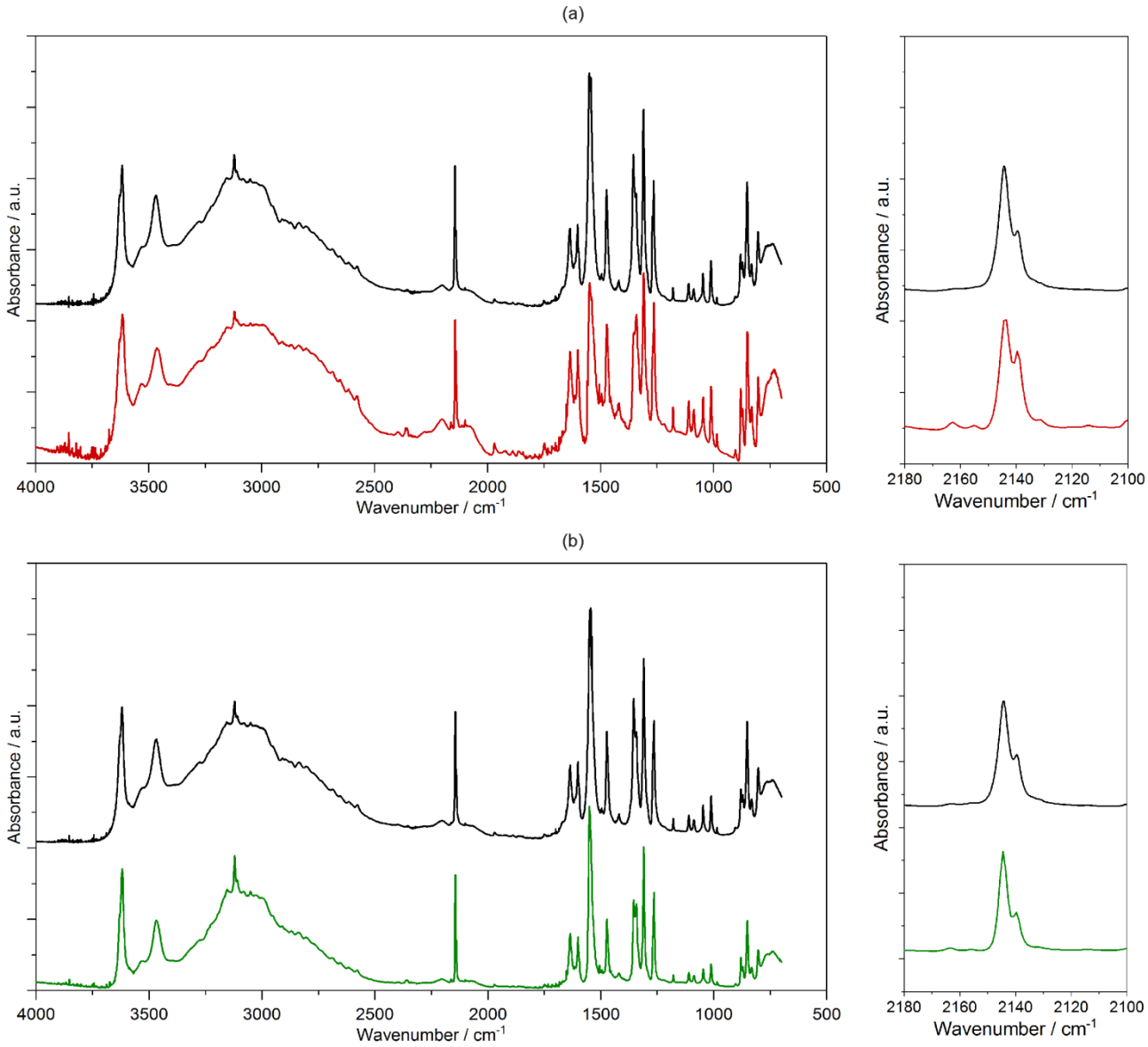

Figure S1 Infrared absorption spectra of **1** (*a*) and **2** (*b*) of the respective polycrystalline samples mixed with potassium bromide (black lines), and of the selected single crystals (coloured lines). The spectra on the left side present the whole wavenumber measurement scope of 4000–700 cm^{-1}, while the smaller graphs on the right side represent the limited range of 2180–2100 cm^{-1}, related to the stretching vibrations of cyanides.

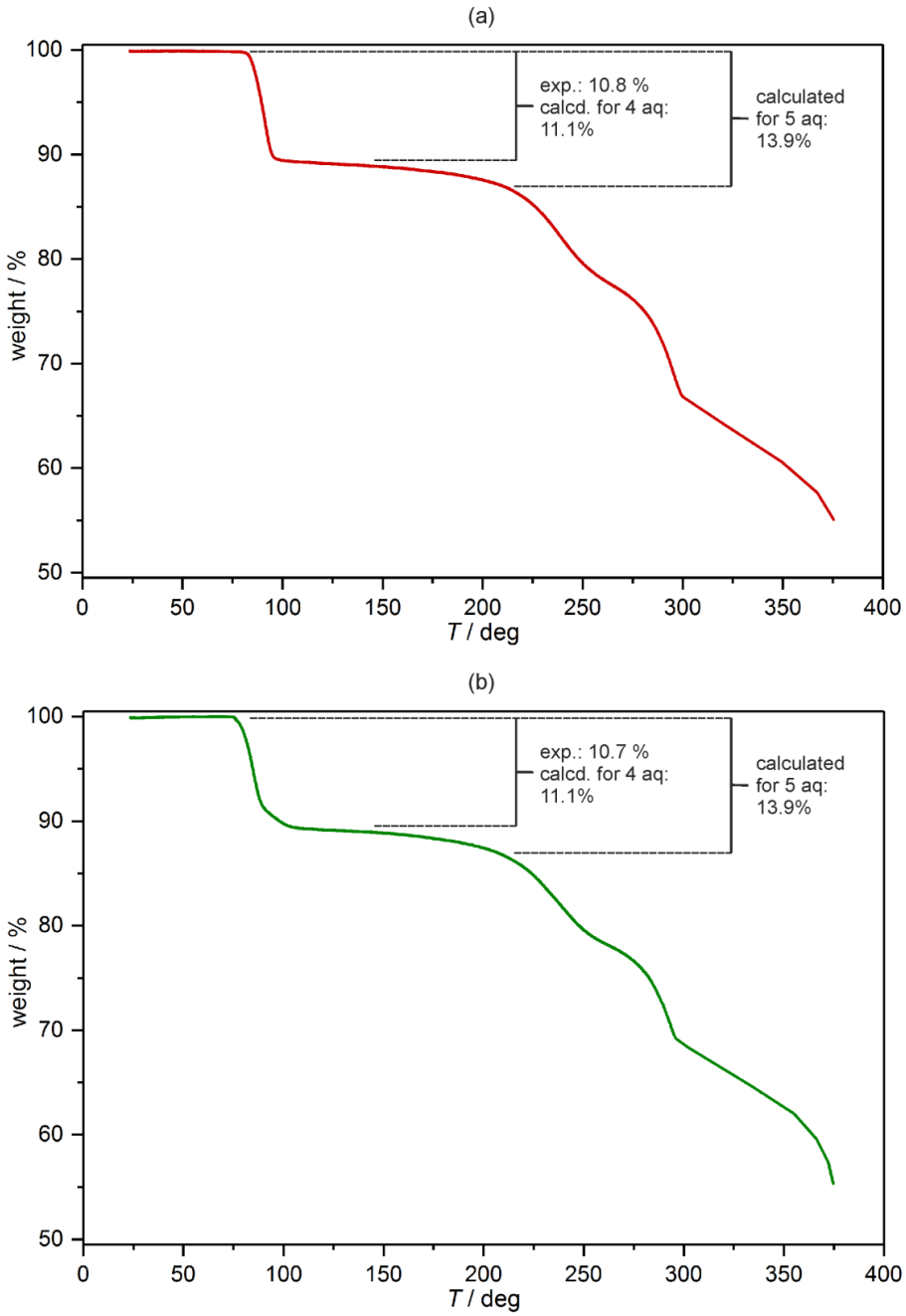

Figure S2 Thermogravimetric curves measured in the temperature range of 20–375 °C of **1** (*a*) and **2** (*b*), with the indicated steps related to the loss of water molecules on a heating process (see the comment on the next page). The experiment was executed under an air atmosphere with the heating rate of 1 °C per minute.

Comment to Figure S2

Under an air atmosphere, the compositions of both **1** and **2** are stable on heating up to 100°C. On further increase of temperature, the weight gradually decreases with a few subsequent steps. Firstly, the rapid mass losses are observed in the narrow ranges of 90–100°C and 90–105°C for **1** and **2**, respectively. The respective decreases of the sample weight are 10.8% and 10.7% in **1** and **2**, respectively. These values correspond well to the mass loss of 11.1% expected for the removal of four water molecules per {LnCr} (Ln = Gd, Tb) unit. It means that at ca. 105°C, **1** and **2** are transformed to partially dehydrated $\{[Ln^{III}(3\text{-pyridone})_2(H_2O)][Cr^{III}(CN)_6]\}$ (Ln = Gd, Cr) with presumably one remaining water molecule within the network. This last water molecule is gradually removing upon further heating in the very broad 100–200°C without the distinguishable step. Just after reaching the fully dehydrated $\{[Ln^{III}(3\text{-pyridone})_2][Cr^{III}(CN)_6]\}$ forms around 200°C, the samples of **1** and **2** become unstable, and further heating leads to the dramatic weight loss related to typical loss of terminal cyanides,[S1] and probable gradual decomposition of 3-pyridone ligands. At the highest available temperature of 375°C, the mass of the residual samples of **1** and **2** is only ca. 55% of the starting room temperature mass.

Such relatively high thermal stability of the compounds **1** and **2**, containing both coordinated and crystallization water molecules, is clearly connected with the strong hydrogen bonding network. Similar behaviour was detected in the analogous and isostructural $\{[Dy^{II}(3\text{-OHpy})_2(H_2O)_4][Co^{III}(CN)_6]\}$ chains,[S2] exhibiting, however, under the identical experimental conditions, the multi-step removal of water molecules starting at a little bit lower temperature around 90°C. It means that the Cr^{III}-containing analogues, **1** and **2**, reveal the improved thermal stability presumably related to the stronger hydrogen bonds within their supramolecular network. Such statement is also supported by the quick removal of the most of water molecules in **1** and **2**, almost in one step, which indicates the significant cooperative effect between hydrogen bonded water molecules in their crystal structures, much stronger than in the {DyCo} chains,[S2] as well as the analogous $\{Eu_xTb_{1-x}Co\}$ coordination polymers.[S3]

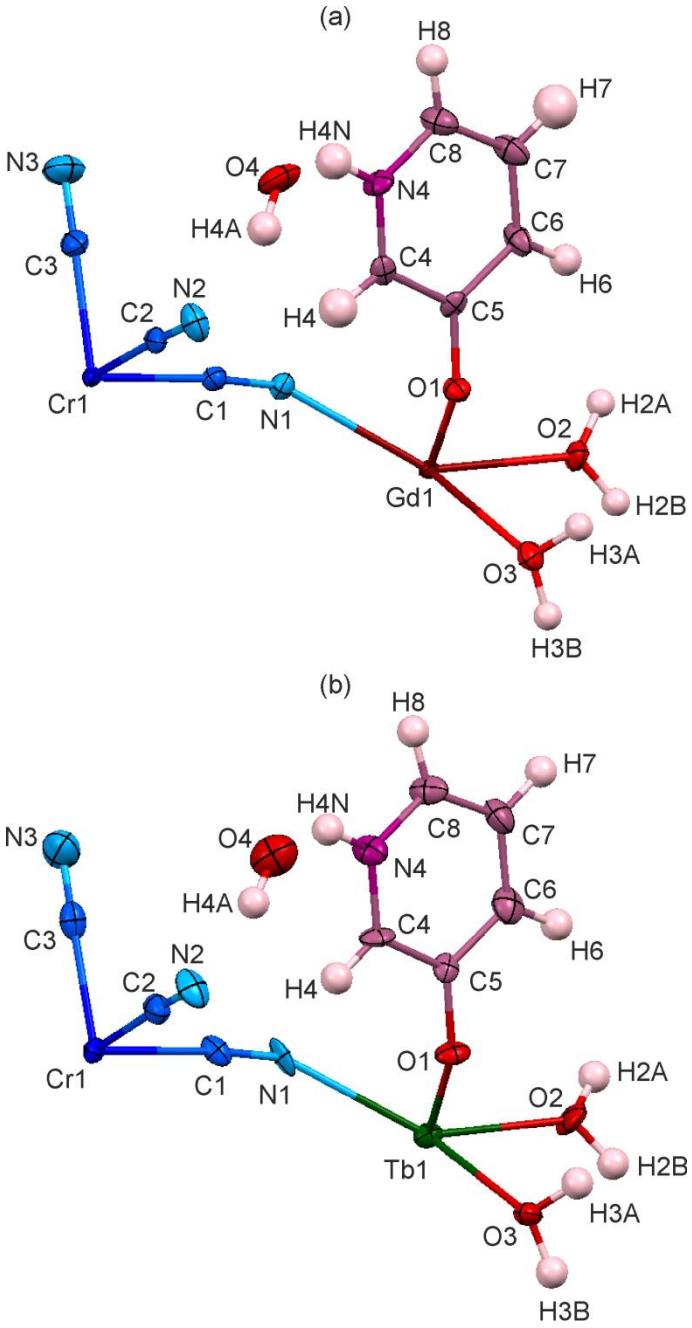

Figure S3 Asymmetric units of **1** (*a*) and **2** (*b*) with the atoms labelling schemes. Thermal ellipsoids are presented at the 60% probability level. The related bond lengths and angles are collected in Table S1.

Table S1 Detailed structure parameters of **1** and **2**.

Details of $[Cr^{III}(CN)_6]^{3-}$ complex			Details of $[Ln^{III}(3\text{-pyridone})_2(H_2O)_4(NC)_2]^{+}$ complex		
Parameter	Value [Å, °]		Parameter	Value [Å, °]	
compound	**1** (Ln = Gd)	**2** (Ln = Tb)	compound	**1** (Ln = Gd)	**2** (Ln = Tb)
Cr1-C1	2.072(4)	2.093(9)	Ln1-N1	2.544(4)	2.528(8)
Cr1-C2	2.072(5)	2.096(9)	Ln1-O1	2.317(3)	2.287(6)
Cr1-C3	2.060(5)	2.067(10)	Ln1-O2	2.406(3)	2.378(6)
C1-N1	1.148(6)	1.135(11)	Ln1-O3	2.439(3)	2.422(6)
C2-N2	1.151(6)	1.129(12)	Ln1-N1-C1	152.1(3)	151.6(7)
C3-N3	1.148(7)	1.148(13)	Ln1-O1-C5	133.8(3)	134.7(5)
Cr1-C1-N1	175.2(4)	175.5(8)	N1-Ln1-N1	75.38(17)	75.3(3)
Cr1-C2-N2	176.8(4)	178.0(9)	O1-Ln1-O1	149.39(15)	149.7(3)
Cr1-C3-N3	177.8(5)	177.9(9)	O2-Ln1-O2	147.09(16)	147.3(3)
C1-Cr1-C1	180	180.0(4)	O3-Ln1-O3	70.01(15)	70.3(3)
C2-Cr1-C2	180	180	N1-Ln1-O1	75.11(11) 80.74(11)	75.6(2) 80.5(2)
C3-Cr1-C3	180	180.00(19)	N1-Ln1-O2	68.76(11) 144.14(11)	68.7(2) 144.0(2)
C1-Cr1-C2	89.30(16) 90.70(16)	89.9(3) 90.1(3)	N1-Ln1-O3	128.67(11) 132.18(11)	128.7(2) 132.1(2)
C1-Cr1-C3	89.85(17) 90.15(17)	89.4(4) 90.6(4)	O1-Ln1-O2	90.43(12) 98.17(11)	90.5(2) 97.9(2)
C2-Cr1-C3	88.82(18) 91.18(18)	88.8(4) 91.2(4)	O1-Ln1-O3	70.67(11) 139.77(11)	70.3(2) 139.8(2)
Cr1-Ln1 distance	5.558	5.550	O2-Ln1-O3	74.13(11) 79.01(11)	74.6(2) 78.8(2)

Table S2 Results of Continuous Shape Measure Analysis for $[Ln^{III}(3\text{-pyridone})_2(H_2O)_4(NC)_2]^+$ complexes in **1** (Ln = Gd) and **2** (Ln = Tb)

Dy complex	CSM parameters			Geometry
	BTP-8	SAPR-8	DD-8	
$[Gd^{III}(3\text{-pyridone})_2(H_2O)_4(NC)_2]^+$ in **1**	2.378	2.392	0.616	**DD-8**
$[Tb^{III}(3\text{-pyridone})_2(H_2O)_4(NC)_2]^+$ in **2**	2.400	2.432	0.626	**DD-8**

Continuous Shape Measure (CSM) parameters:[S4-S5]

CSM BTP-8 = the parameter related to the bicapped trigonal prism geometry (C_{2v} symmetry)

CSM SAPR-8 = the parameter related to the square antiprism (D_{4d} symmetry)

CSM DD-8 = the parameter related to the dodecahedron (D_{2d} symmetry)

CSM = 0 for the ideal geometry and the increase of CSM parameter corresponds to the increasing distortion from the ideal polyhedron.

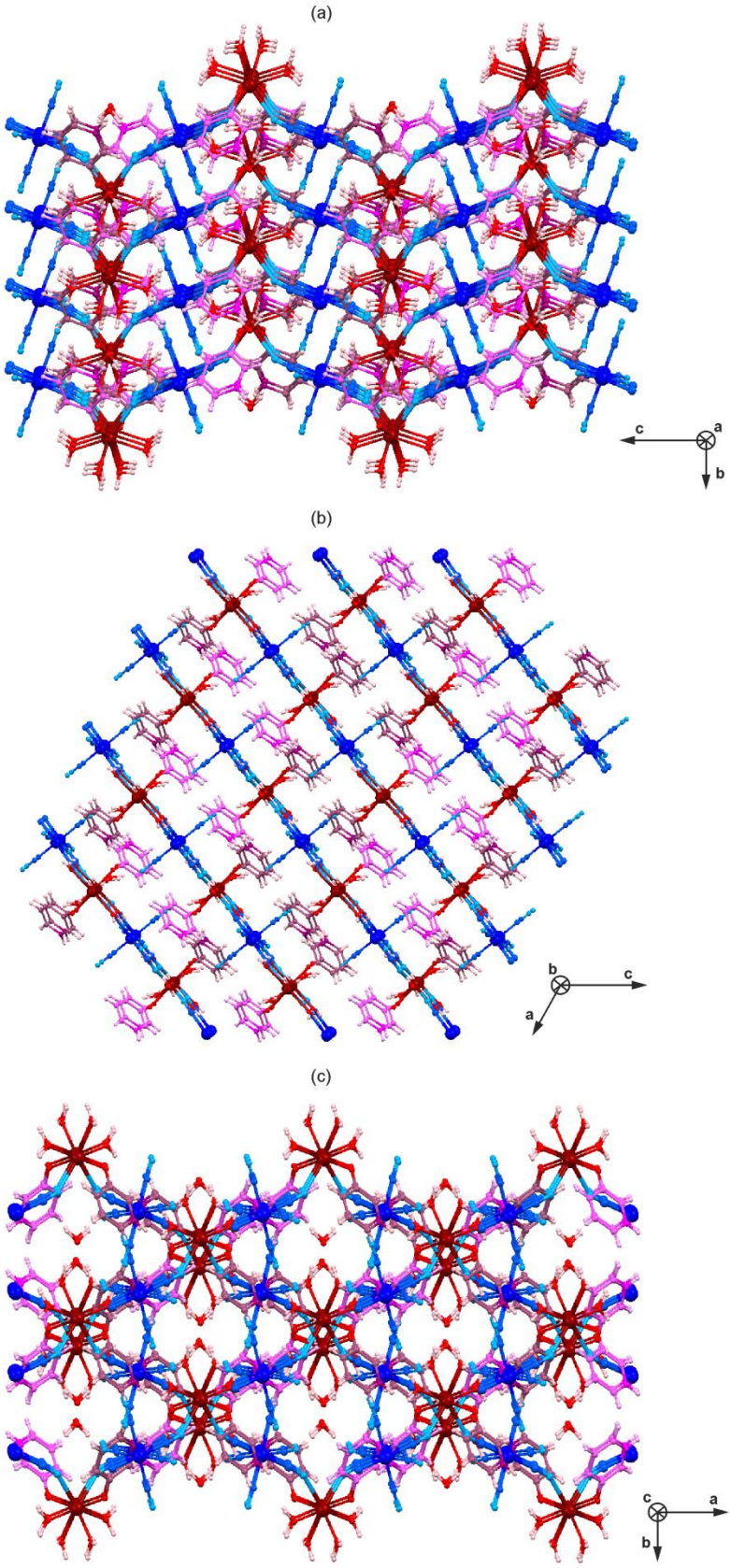

Figure S4 The views of the supramolecular network of **1** along the ***a*** (*a*), ***b*** (*b*), and ***c*** (*c*) crystallographic axes. Colours: Gd, dark red; Cr, dark blue; O, red, C of cyanides, blue; N of cyanide, light blue; 3-pyridone ligands, light purple and magenta; H, pinkish.

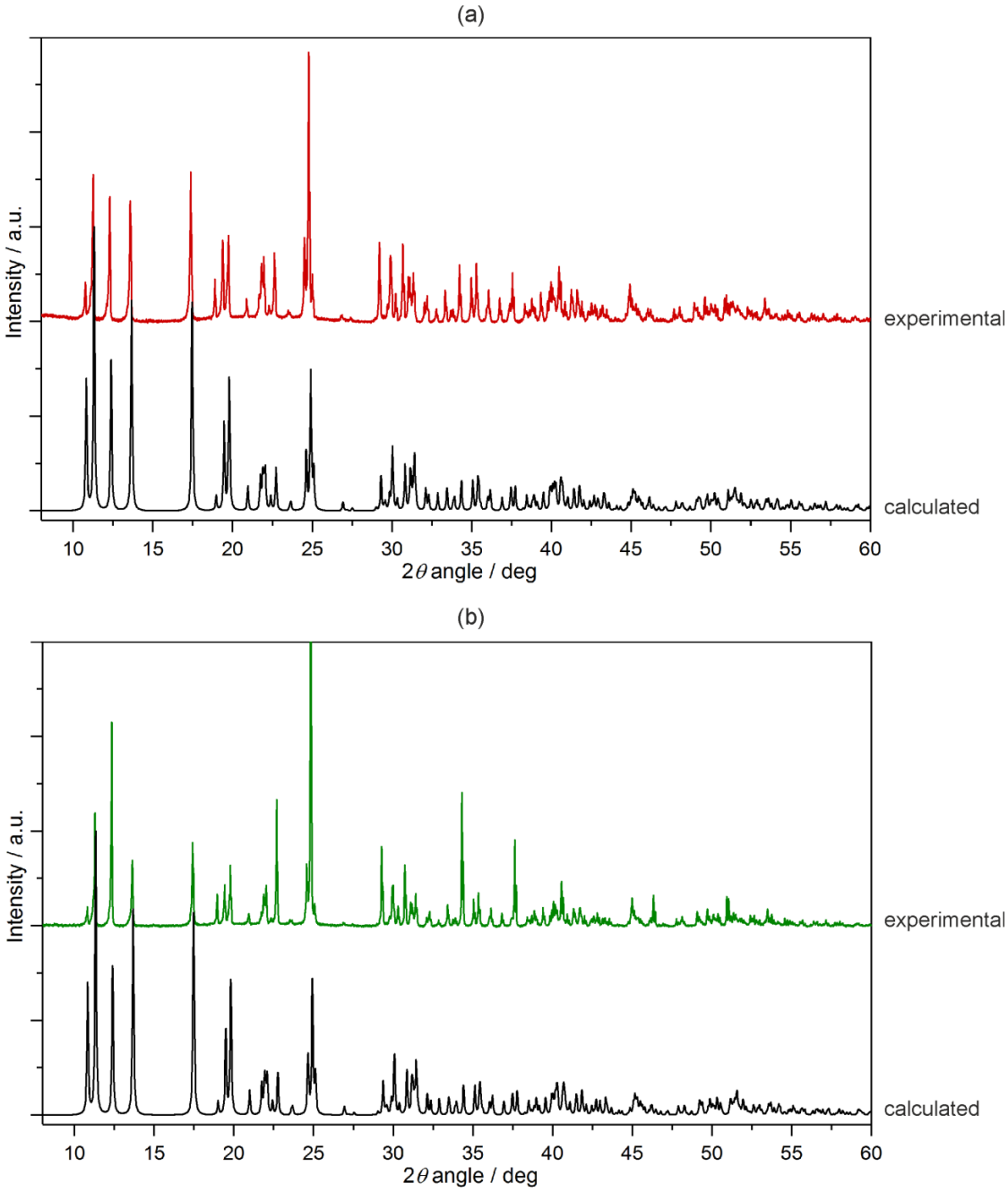

Figure S5 Experimental powder X-ray diffraction (PXRD) patterns of the polycrystalline samples of **1** (*a*) and **2** (*b*) compared with the patterns calculated from the respective structural models obtained from the single-crystal X-ray (SC-XRD) structural analyses. The representative range of 8–60° of 2Θ angle is presented. The consequent small shift of all the diffraction peaks is caused by the standard temperature effect, as the PXRD measurement was performed at room temperature when the SC-XRD experiment was done at the low temperature of 120(2) K.

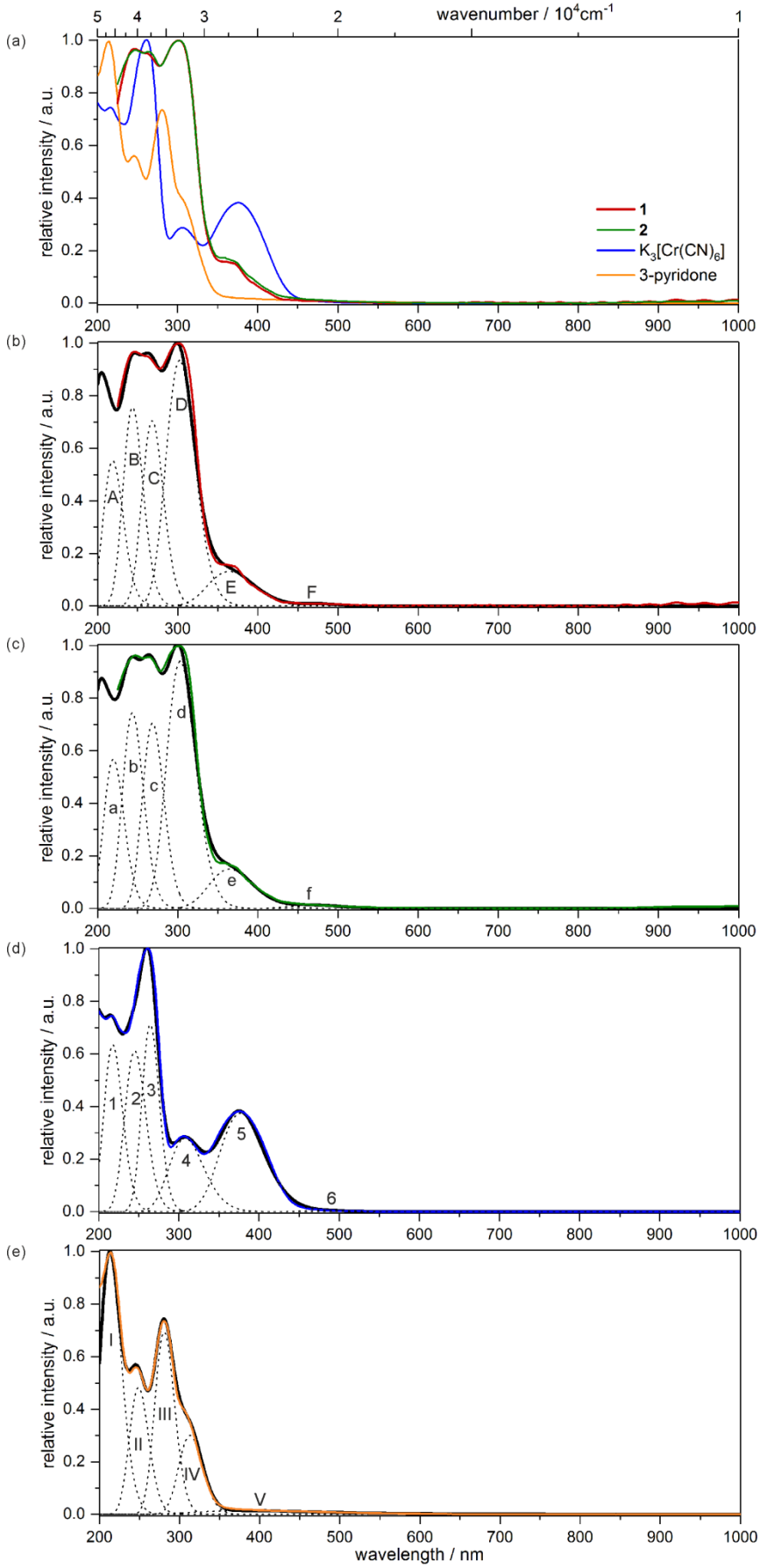

Figure S6 Solid-state UV-Vis-NIR absorption spectra of **1** (*a*,*b*) and **2** (*a*,*c*) compared with the relevant spectra of $K_3[Cr(CN)_6]$ (*a*,*d*) and 3-pyridone (*a*,*e*). The colour solid lines are the experimental data (225–1000 nm range), the dotted lines are the components of the UV-Vis-NIR bands (Table S3), and the black solid lines are the respective calculated sums (200–1000 nm range).

Table S3 Analysis of solid state UV-Vis-NIR absorption spectra of **1** and **2** compared with the analyses of the relevant spectra of $K_3[Cr(CN)_6]$ and 3-pyridone (see Figure S6).

compound (figure)	peak no.	λ_{max} / nm	E_{max} / cm^{-1}	interpretation
1 (figure S6b)	A	219	45700	combined contributions from charge transfer transitions within the $[Cr^{III}(CN)_6]^{3-}$ moiety, and singlet to singlet transitions of 3-pyridone ($\pi \rightarrow \pi^*$)
	B	243	41050	
	C	268	37300	
	D	302	33080	combined contributions from d–d transition of Cr^{III}: $^4A_{2g} \rightarrow {}^4T_{1g}$, and singlet to singlet transitions of 3-pyridone ($\pi \rightarrow \pi^*$)
	E	364	27450	combined contributions from d–d transition of Cr^{III}: $^4A_{2g} \rightarrow {}^4T_{2g}$, and singlet to triplet transitions of 3-pyridone ($\pi \rightarrow \pi^*$)
	F	478	20900	d–d transition of Cr^{III}: $^4A_{2g} \rightarrow {}^2T_{2g}$
2 (figure S6c)	a	220	45540	combined contributions from charge transfer transitions within the $[Cr^{III}(CN)_6]^{3-}$ moiety, and singlet to singlet transitions of 3-pyridone ($\pi \rightarrow \pi^*$)
	b	244	41090	
	c	269	37240	
	d	303	33010	combined contributions from d–d transition of Cr^{III}: $^4A_{2g} \rightarrow {}^4T_{1g}$, and singlet to singlet transitions of 3-pyridone ($\pi \rightarrow \pi^*$)
	e	365	27420	combined contributions from d–d transition of Cr^{III}: $^4A_{2g} \rightarrow {}^4T_{2g}$, and singlet to triplet transitions of 3-pyridone ($\pi \rightarrow \pi^*$)
	f	472	21200	d–d transition of Cr^{III}: $^4A_{2g} \rightarrow {}^2T_{2g}$
$K_3[Cr(CN)_6]$ (figure S6d)	1	217	46080	charge transfer transitions between Cr^{III} and cyanide ligands, both ligand-to-metal (lower energy) and metal-to-ligand (higher energy)[S6-S8]
	2	245	40820	
	3	264	37880	
	4	308	32470	d–d transition of Cr^{III}: $^4A_{2g} \rightarrow {}^4T_{1g}$
	5	377	26530	d–d transition of Cr^{III}: $^4A_{2g} \rightarrow {}^4T_{2g}$
	6	485	20620	d–d transition of Cr^{III}: $^4A_{2g} \rightarrow {}^2T_{2g}$
3-pyridone (figure S6e)	I	213	46950	singlet to singlet transitions:[S2,S9-S10] $\pi \rightarrow \pi^*$
	II	249	40160	
	III	281	35600	
	IV	313	31950	
	V	385	26000	singlet to triplet transition: $\pi \rightarrow \pi^*$

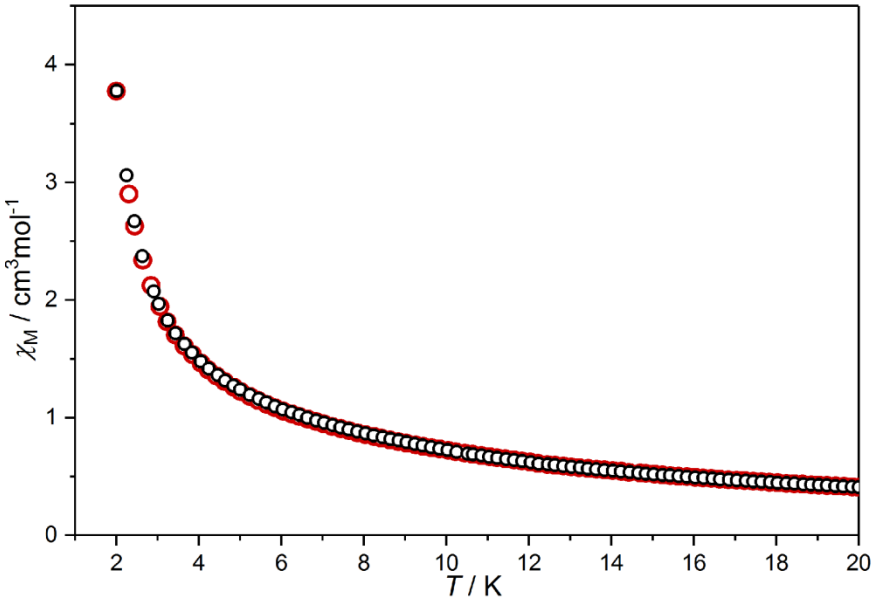

Figure S7 Zero-field-cooled (ZFC, red points) and field-cooled (FC, black points) magnetic susceptibility curves under an applied *dc* magnetic field of 15 Oe in the 1.8–20 K range for **1**.

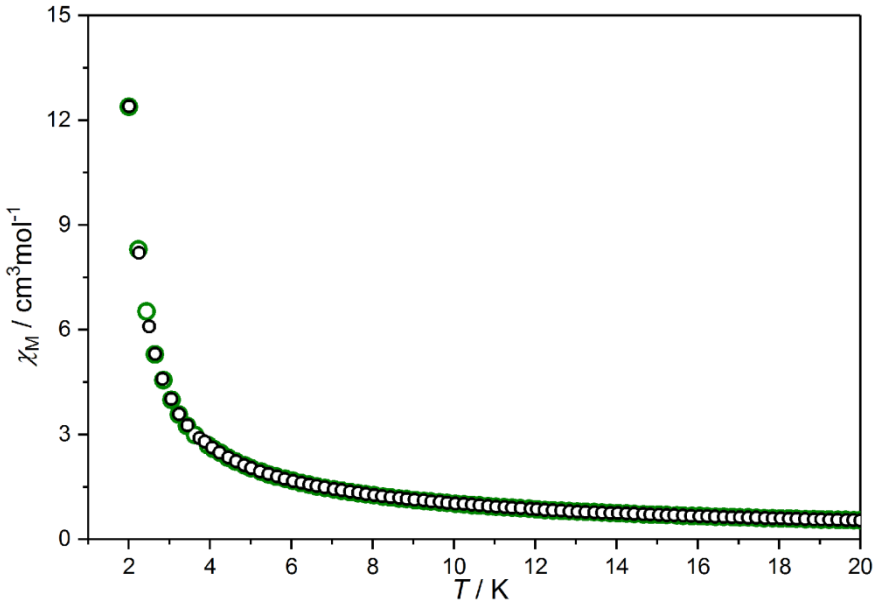

Figure S8 Zero-field-cooled (ZFC, red points) and field-cooled (FC, black points) magnetic susceptibility curves under an applied *dc* magnetic field of 15 Oe in the 1.8–20 K range for **2**.

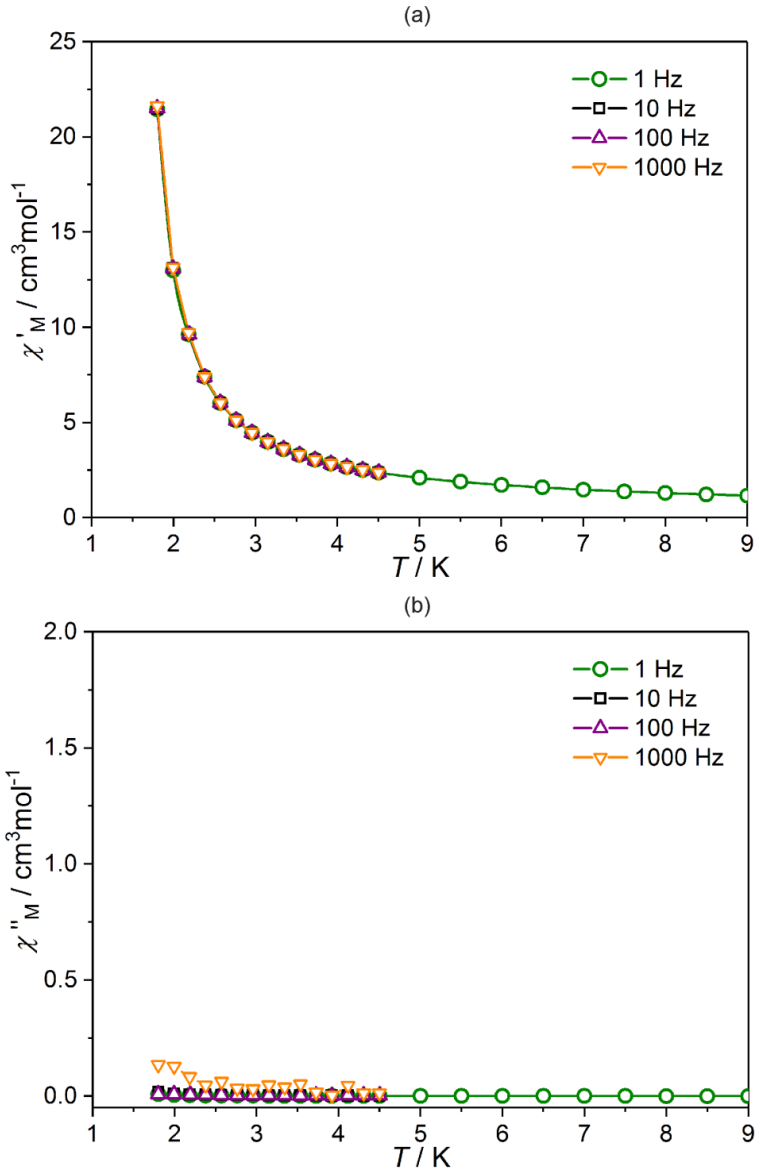

Figure S9 Temperature dependences of the in-phase, χ'_M (*a*), and out-of-phase, χ''_M (*b*) molar magnetic susceptibilities of **2**, under various indicated frequencies of the *ac* magnetic field. Magnetic field conditions: H_{dc} = 0 Oe; H_{ac} = 3 Oe.

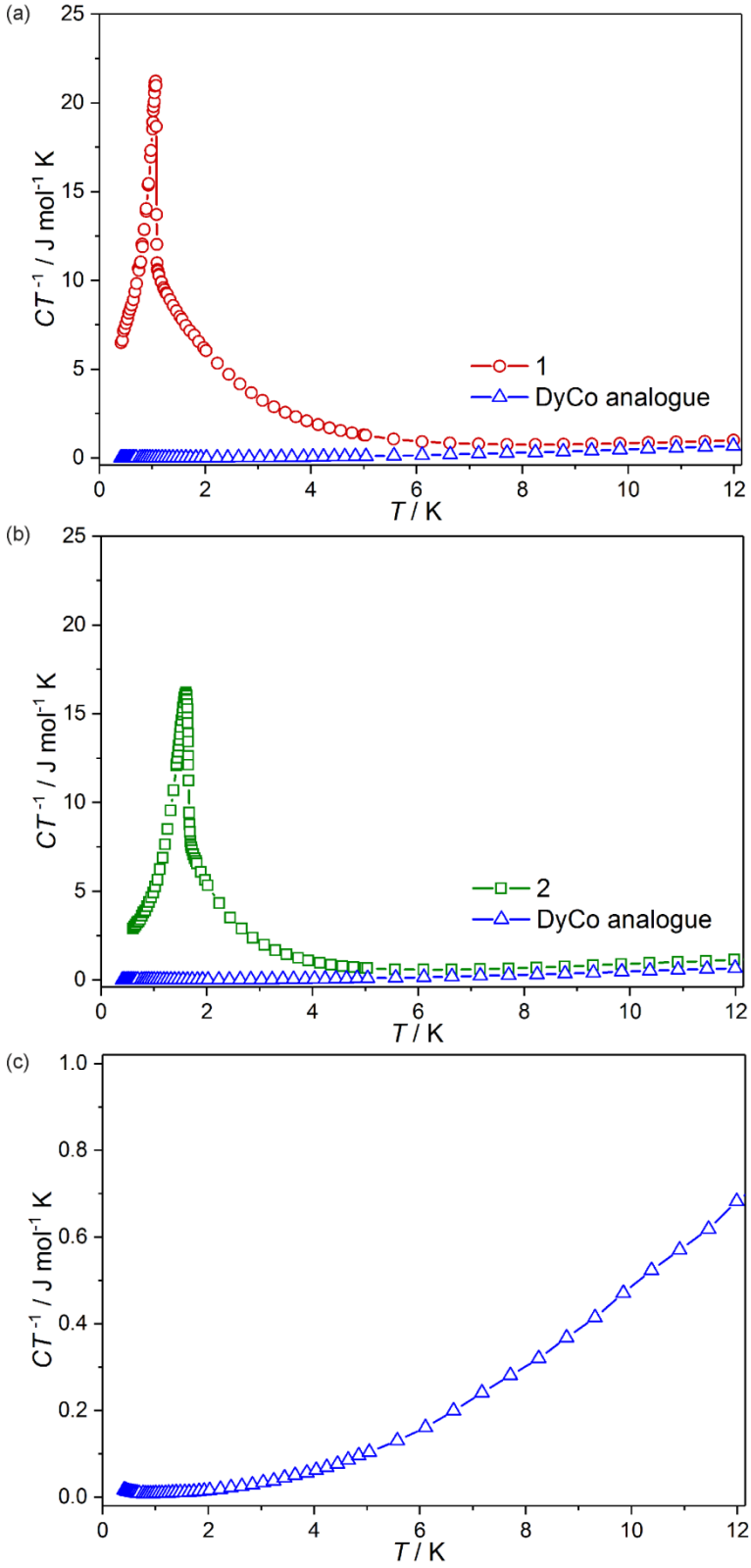

Figure S10 Temperature dependences of total heat capacity of **1** (*a*) and **2** (*b*) compared with the analogous $\{[Dy^{II}(3\text{-}OHpy)_2(H_2O)_4][Co^{III}(CN)_6]\}\cdot H_2O$ chains, which exhibit the paramagnetism without magnetic coupling and magnetic ordering due to the presence of diamagnetic $[Co^{III}(CN)_6]^{3-}$ ions. This material was prepared according to the published procedure.[S2] In addition, the detailed view of the heat capacity versus temperature curve for the DyCo analogue was presented in the (*c*) part. It was used to subtract the phonon contribution to the heat capacity resulting in the magnetic heat capacity curves shown in the manuscript (Figure 6).

References to Supporting Information

[S1] S. Chorazy, K. Nakabayashi, M. Arczyński, R. Pełka, S. Ohkoshi and B. Sieklucka, *Chem. Eur. J*., 2014, **20**, 7144.

[S2] S. Chorazy, M. Rams, K. Nakabayashi, B. Sieklucka and S. Ohkoshi, *Chem. Eur. J*., 2016, **22**, 7371.

[S3] S. Chorazy, K. Kumar, K. Nakabayashi, B. Sieklucka and S. Ohkoshi, *Inorg. Chem*., 2017, **56**, 5239.

[S4] M. Llunell, D. Casanova, J. Cirera, J. Bofill, P. Alemany, S. Alvarez, M. Pinsky, D. Avnir, *SHAPE v. 2.1. Program for the Calculation of Continuous Shape Measures of Polygonal and Polyhedral Molecular Fragments*, University of Barcelona: Barcelona, Spain, 2013.

[S5] D. Casanova, J. Cirera, M. Llunell, P. Alemany, D. Avnir and S. Alvarez, *J. Am. Chem. Soc*., 2004, **126**, 1755.

[S6] J. J. Alexander and H. B. Gray, *J. Am. Chem. Soc*., 1968, **90**, 4260.

[S7] L. Aboshyan-Sorgho, M. Cantuel, S. Petoud, A. Hauser and C. Piguet, *Coord. Chem. Rev*., 2012, **256**, 1644.

[S8] S. Chorazy, B. Sieklucka and S. Ohkoshi, *Cryst. Growth Des*., 2016, **16**, 4918.

[S9] A. Weisstuch, P. Neidig and A. C. Testa, *J. Lumin*., 1975, **10**, 137.

[S10] O. K. Abou-Zied and O. I. K. Al-Shihi, *Phys. Chem. Chem. Phys*., 2009, **11**, 5377.